Terraforming Mars:
Solutions to Shield against Cosmic Radiation

Viktor Lack, 6g
Kantonsschule Wiedikon
Zurich 2023
Supervised by Magnus Gienal

Abstract

In the process of terraforming Mars, cosmic radiation presents a significant problem due to long-term detrimental effects on human, animal, and plant biology. Moreover, it threatens to dissipate any artificial atmosphere on the planet. This paper presents three approaches to establishing a planetary magnetic field to protect Mars from cosmic rays: reactivating Mars's dynamo, a plasma torus around Mars, and electromagnets. Each approach is evaluated for its feasibility and energy requirement. We find that the most feasible solution is an electromagnet made of yttrium barium copper oxide, or possibly pure copper, around the circumference of Mars. The plasma torus is potentially also viable. Reactivating Mars's dynamo is infeasible due to the enormous logistical and energy demands.

Table of Contents

1 Introduction

The exploration and colonization of other planets has long fascinated humanity and led to great scientific discovery and innovation. It is even considered imperative for humanity's long-term survival in the face of existential threats, which include natural disasters such as supervolcanic eruptions and asteroid impacts as well as man-made catastrophes involving nuclear or bioweapons. The planet Mars has stood at the center of these ambitions due to its proximity to Earth and somewhat favorable habitability conditions; NASA is speaking of the 2030's as an optimistic goal for sending the first humans to Mars [1], and Elon Musk, founder and CEO of SpaceX, has envisioned permanent settlements of a million inhabitants on Mars by the 2050's [2]. A next step could be its terraforming: a process which aims to alter a planet's environment to make it more similar to Earth and allow human, animal, and plant habitation without any survival equipment such as spacesuits, special habitats etc. Birch [3], for example, provides a comprehensive overview of some important steps such as how we could warm the planet, create a breathable and dense atmosphere, and import water. Another crucial factor in the terraforming of Mars will be the focus of this paper: radiation protection. Since Mars does not have a global magnetic field like Earth [4], it is exposed to high-energy charged particle beams from space, i.e. cosmic radiation or cosmic rays. This is problematic because radiation damages the biology of life and disperses any existing atmosphere over the long-term. A breathable, dense atmosphere, like the one on Earth, would also protect Mars from harmful electromagnetic (especially UV) waves.

Acute effects of exposure to energetic particle radiation on the human central nervous system (CNS) are fatigue, detriments in short-term memory, behavior changes, and a decrease in performance. Other adverse effects include nausea, vomiting, cataract formation, and in extreme cases skin burning and death. Late radiation morbidity is induced by continual exposure to radiation and leads to increased cancer risk, damage to the CNS, and possibly increased risk for cardiovascular disease [e.g. 5, 6]. Specifically, some models predict an equivalent radiation dose of 1.0 mSv per day on the surface on Mars during solar energetic particle events. Surprisingly, this number is still well below all NASA's guidelines if we consider only a 30 day stay [7]. However, what is hazardous is the cumulative long-term radiation damage during a permanent stay [7], which will result in life-threatening late radiation morbidity. Such long-term low dose radiation exposure also has adverse effects on plants. In general, these are elevated rates of genetic damage including mutations, slower growth rates, decreased fertility, and developmental abnormalities [8].

Mars likely used to have a denser atmosphere until the cessation of its global magnetic field when a process called sputtering likely contributed to its erosion, whereby O^+ ions in the uppermost atmosphere are accelerated by interactions with the solar wind, colliding with other particles and causing them to escape [9, 10]. A magnetic shield is consequently needed to prevent the precipitating ions from eroding a dense artificial atmosphere, which is moreover a requirement for the existence of liquid water on the surface of a terraformed Mars: mean surface pressure is 6.1 millibars [11], less than 1% of 1 atm, under which condition liquid water boils if we assume air temperature is already Earth-like.

The terraforming of Mars must therefore solve these problems. This paper will explore and comment on three approaches to shielding all of Mars from cosmic radiation by means of an artificial planetary magnetic field, detailing their operational mechanism, calculating approximate energy requirements, and contemplating technological prerequisites. Finally, the feasibility of the presented methods will be compared and evaluated and possible applications for current space travel will be considered. However, first of all, the theory section will present the underlying physics as well as some important preliminary calculations about the requirements for the artificial magnetosphere.

2 Theory

2.1 The Fundamentals of Magnetism

To follow the lines of argument in this paper, it is useful to understand the basic concepts of magnetism, of which this section provides a brief overview. The content presented here draws primarily from *College Physics* [12] and *Physik: Lehr- und Übungsbuch* [13].

All magnets consist of one north magnetic pole and one south magnetic pole. Similar to positive and negative charges in electrostatics, unlike poles attract and like poles repel. However, the two poles of a magnet cannot be separated, different from how opposite charges may be separated. Consequently, if one were to halve a bar magnet (see Figure 1), two new magnets would be produced, each with its own north and south pole. The existence of a magnetic monopole is not explicitly forbidden by the laws of physics but has never been observed.

Analogous to the electric field, the magnetic field, or the B-field, is defined to describe the forces exerted by a magnet. We can represent the magnetic field using field lines: the direction of the field is tangential to the lines and their density is proportional to magnetic field strength. A property of magnetic field lines is that they are always continuous, i.e., they always form closed loops, unlike electric field lines. Intuitively, one can make sense of this because a beginning and end point would imply a magnetic monopole, similar to how electric field lines start at the positive charge and end at the negative charge in an electric dipole (see Figure 2).

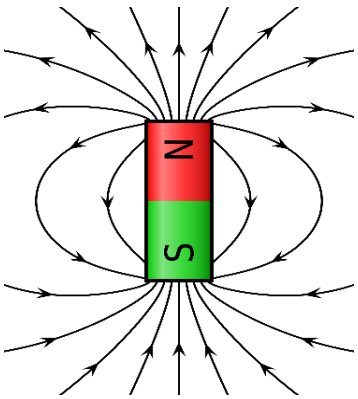

Figure 1: Magnetic field of a cylindrical bar magnet visualized with magnetic field lines. Note that the lines actually continue along the same direction within the magnet and thus form continuous, closed loops.

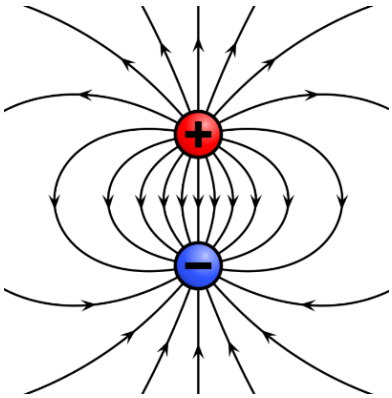

Figure 2: Electric field generated by an electric dipole.

Experiments have shown that a magnet exerts a force on an electric current, as first observed by physicist H. C. Ørsted. The force is described by the following equation:

$$d\vec{F} = I\left(d\vec{s} \times \vec{B}\right) \tag{2.1}$$

where $d\vec{F}$ is an infinitesimal force vector acting upon a current I in a segment $d\vec{s}$. $d\vec{s}$ points in the direction of the current. $\vec{B}$ is the magnetic field at $d\vec{s}$. Integrating $d\vec{F}$ over a current segment results in the net force on the current. In the case of a straight current-carrying conductor in a uniform magnetic field, this means that:

$$\vec{F}_{net} = I(\vec{s} \times \vec{B}) \tag{2.2}$$

Since a current is equivalent to the motion of electrically charged particles, the above force must be the sum of smaller forces on individual particles. One such small force is called the magnetic force and is given by:

$$\vec{F} = q\vec{v} \times \vec{B} \tag{2.3}$$

where q is the electric charge of the particle and $\vec{v}$ its velocity. The definition of $\vec{B}$, that is its direction and magnitude at any point in space, hinges on equation 2.1 or 2.3: $\vec{B}$ is precisely the vector that satisfies these equations. The unit of $|\vec{B}|$ is therefore $\frac{\mathrm{N}}{\mathrm{A{\cdot}m}}$ or a Tesla (T). A Tesla is also equal to 10^4 Gauss (Gs).

We have seen how a magnet exerts a force on a current. Due to Newton's third law, one would expect that a current exerts a reactionary force back on the magnet. That is indeed the case, and it implies that the current generates a magnetic field through which this reactionary force is communicated. The nature of this magnetic field is mathematically describable. Ampère's law is the most fundamental relation this paper will show:

$$\oint \vec{B} \cdot d\vec{s} = \mu_0 \cdot I_{encl} \tag{2.4}$$

where $\oint \vec{B} \cdot d\vec{s}$ is the closed path integral of the dot product of the B-field with an infinitesimal segment of the path $d\vec{s}$. The right-hand side contains I_{encl}, which is the current enclosed by the chosen integration path. μ_0, the permeability of free space, is a constant with a value approximately equal to $4\pi \cdot 10^{-7}$ $\frac{\mathrm{N}}{\mathrm{A}^2}$. In fact, until 2019, μ_0 was by definition $4\pi \cdot 10^{-7} \frac{\mathrm{N}}{\mathrm{A}^2}$, and the Ampère was defined by the implications of equation 2.4, but now, the elementary charge e is fixed and μ_0 must be experimentally determined [14]. Ampère's law does not hold when magnetic materials are involved, or the magnetic field and currents are not stationary.

To illustrate how one would work with this equation, the magnetic field for a long straight wire carrying current I (see Figure 3) is derived: The integration path is chosen to be a circle with radius r. The wire passes through the circle's center at a right angle with r. Due to symmetry, we expect $\vec{B}$ to have the same magnitude everywhere on the integration path. Furthermore, we will rightly assume that $\vec{B}$ is tangential to the circle and that the angle between $\vec{B}$ and $d\vec{s}$ is therefore 0. This gives:

$$\mu_0 \cdot I = \oint \vec{B} \cdot d\vec{s} = \oint B\, ds = B \cdot \oint ds = B \cdot 2\pi r \tag{2.5}$$

where I is I_{encl} and the $\oint ds$ is just the circumference of the circle. Solving for B:

$$B = \frac{\mu_0 I}{2\pi r} \tag{2.6}$$

Ampère's law is limited in the sense that computing B is only possible when the problem exhibits a symmetry which allows B to be taken out of the integral. The Biot-Savart law, on the other hand, directly computes $\vec{B}$ at a certain point in space defined by position vector $\vec{r}$:

$$\vec{B}(\vec{r}) = \frac{\mu_0}{4\pi} \int_C \frac{I(d\vec{l} \times \check{\vec{r}}')}{|\vec{r}'|^2} \tag{2.7}$$

$\vec{B}$ is given by a constant, $\frac{\mu_0}{4\pi}$, multiplied by an integral over the current-carrying conductor C, such as a wire. The current I in C generates the magnetic field. In the integral, $d\vec{l}$ signifies an infinitesimal segment of the conductor and points in the direction of the conventional current I. $\vec{r}'$ is the connecting vector from $d\vec{l}$ to the position indicated by $\vec{r}$, and $|\vec{r}'|^2$ is its norm squared. $\check{\vec{r}}'$ points in the same direction as the connecting vector $\vec{r}'$ but has norm 1. This equation is powerful because it allows us to compute $\vec{B}$ at arbitrary positions. However, theoretically, one would have to account for all currents everywhere in space, which is why calculations for an estimate become very complex as soon as multiple currents are nearby.

After brief examination, the law may reveal the direction of the magnetic field in some cases. Consider, for instance, the magnetic field due to a straight wire in Figure 3. The Biot-Savart law integrates a vector $d\vec{l} \times \check{\vec{r}}'$. Because this is a cross product, the resulting infinitesimal vector will always point perpendicular to I and $\check{\vec{r}}'$, which means, in our case, that it is tangential to the circular field lines, and it will follow the right-hand rule. The integral of the infinitesimal vectors is therefore also tangential to the field lines and follows the right-hand rule.

The Biot-Savart law can be used to derive the magnitude of the magnetic field on the axis of a conducting loop (Figure 4):

$$B = \frac{\mu_0 I r^2}{2(r^2 + x^2)^{\frac{3}{2}}} \tag{2.8}$$

where r is the loop radius and x is distance from the center of the loop. When $x \gg r$, the following is roughly accurate:

$$B \propto \frac{1}{x^3} \tag{2.9}$$

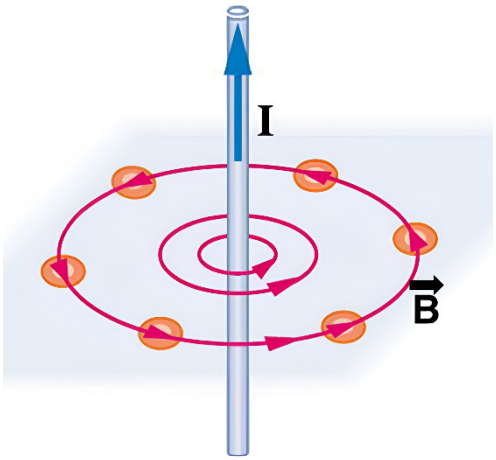

Figure 3: Magnetic field generated by a current in a straight wire. The right-hand rule describes the direction of $\vec{B}$: if the thumb points in the same direction as I*, the fingers follow $\vec{B}$.*

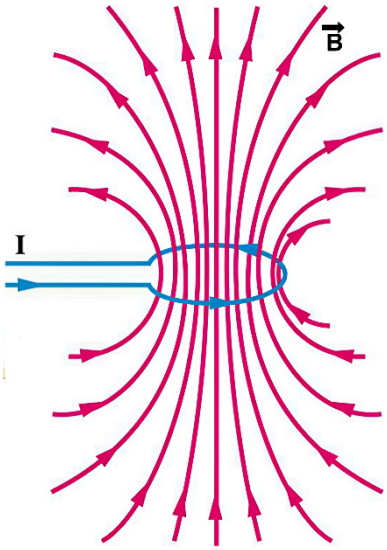

Figure 4: The magnetic field of a current loop. The magnetic field lines follow the right-hand rule again.

It turns out that this relation also holds for points which do not lie on the loop's axis, just with different proportionality factors (which we will neglect in this paper for simplicity). Bar magnets exhibit the same behavior as in relation 2.9; observe the similarity between the fields in Figure 1 and Figure 4. It makes sense that current loops are considered magnetic dipoles like bar magnets.

The reasoning behind 2.9 is the following: if we let the dipole's radius r approach zero but keep its magnetic moment $m = I\pi r^2$ constant, which results in an ideal magnetic dipole with infinite current and zero area, the relation is exactly true (from taking the limit in equation 2.8). Now acknowledge that observed over a sufficiently large scale, bar magnets and current loops approximate an ideal dipole.

The significance of 2.9 reveals itself when considering the ratio between magnetic field strength at different distances x_0 and x_1 from the dipole:

$$\frac{B(x_1)}{B(x_0)} \approx \frac{cx_1^{-3}}{cx_0^{-3}} = \frac{x_0^3}{x_1^3} \tag{2.10}$$

where c is a proportionality factor specific to the dipole in question (see equation 2.8). In other words:

$$B(x_1) \approx \left(\frac{x_0}{x_1}\right)^3 \cdot B(x_0) \tag{2.11}$$

2.2 Requirements for Planetary Magnetic Field Strength

To produce an estimate of the necessary magnetic field strength, ram pressure P_{ram} from cosmic rays and magnetic pressure given by $\frac{B^2}{2\mu_0}$ are equated. DuPont and Murphy [15] start off with the same equation:

$$P_{ram} = \frac{B(r_S)^2}{2\mu_0} \tag{2.12}$$

where μ_0 is the permeability of free space, and r_S the stand-off distance from the planet's center, i.e., the distance for which the above equation holds since B is a function of r_S. At the stand-off distance, the magnetic field will deflect charged particles originating from the Sun and outside the solar system because the pressure P_{ram} they exert is counterbalanced. In a planetary context, this boundary is called the magnetopause.

Ram pressure may be expressed as ρv^2, where ρ is density and v is particle velocity, in the simple case of the radiation fully transferring its momentum to the magnetic shield. Therefore, equation 2.12 becomes:

$$\rho v^2 = \frac{B(r_S)^2}{2\mu_0} \tag{2.13}$$

For this calculation, only radiation from the Sun (solar wind) will be considered due to its much greater density compared to galactic or even extragalactic cosmic rays.

Dynamic solar radiation pressure at 1 AU, i.e. near Earth's orbit, averages ~2 nPa but may vary greatly depending on solar activity, reaching 60 nPa on January 11th, 1997 [16], for example. However, radiation pressure may be much greater during coronal mass ejections (CMEs), which belong to the Sun's

most energetic events. CMEs are characterized by notable ejection of plasma mass and magnetic fields. Even during minimal solar activity, they occur at least once every few days [17]. Average particle velocities range from 300 to 500 km·s^{-1} but reach more than 1500 km·s^{-1} in ~0.5% of cases [18]. The fastest CME was measured on January 20th, 2005, to be 3675 km·s^{-1} [18]. Maximum particle number density lies around 200 cm^{-3} [18]. It is reasonable to proceed our calculations with a velocity of 3000 km·s^{-1}, a number density of 200 cm^{-3}, and a composition of solely protons, instead of a mix of protons and electrons, for a conservative estimate of required field strength; ρ is expressed as the product of number density (200 cm^{-3}) and proton mass (taken from [19]). Maximum ram pressure near Earth's orbit assumes 3.0 µPa or 3000 nPa using these values, according to the left-hand term of equation 2.13.

DuPont and Murphy [15] now use a clever way to relate solar wind pressure near Earth's orbit to pressure near Mars's orbit: $\dot{M}$ describes the Sun's mass loss due to solar wind over time and can be reformulated using dimensional analysis:

$$\dot{M} = \frac{\rho V}{\Delta t} = \rho v A = \rho v 4\pi D^2 \tag{2.14}$$

where D is the distance from the center of the Sun. Because $\dot{M}$ and v will be assumed to be constant, this means that $\rho \propto \frac{1}{D^2}$. This paper cites Elliott et al. [20] for reference, who confirm this given that solar wind is analyzed in large datasets. For smaller parcels of particles, however, this description is insufficient due to local compression or rarefaction, but it will suffice to relate ram pressure near the orbits of Earth and Mars. Ram pressure as a function of distance is, therefore:

$$P_{ram}(D) = \frac{\dot{M}}{\rho v 4\pi D^2}\rho v^2 = \frac{\dot{M} v}{4\pi D^2} \tag{2.15}$$

Then, as one would already expect from the inverse square relation of density:

$$P_{ram,M} = \frac{\dot{M} v}{4\pi \left(D_E \cdot \frac{D_M}{D_E}\right)^2} = \frac{\dot{M} v}{4\pi {D_E}^2} \cdot \left(\frac{D_E}{D_M}\right)^2 = P_{ram,E} \cdot \left(\frac{D_E}{D_M}\right)^2 \tag{2.16}$$

where D_E is distance from the center of the Sun to Earth's orbit and D_M is distance to Mars's orbit. $P_{ram,M}$ and $P_{ram,E}$ represent ram pressure near Mars's and Earth's orbit, respectively. A reasonable estimate for maximum ram pressure near Mars's orbit is:

$$P_{ram,M,max} \approx 3.0 \cdot \left(\frac{1.0}{1.5}\right)^2 \approx 1.3 \text{ µPa}$$

where we used maximum ram pressure near Earth's orbit of 3.0 µPa. The ratio between the distances $\frac{D_E}{D_M} \approx \frac{1.0}{1.5}$ comes from [19]. Returning to equation 2.12, $B(r_S)$ must be around 1.8 µT to defy this pressure. DuPont and Murphy [15] approached the calculation of $B(r_S)$ differently by using a comparison to Earth's stand-off distance, but us working with concrete values for ram pressure is more accurate considering that r_S is not constant, neither for Earth nor a terraformed Mars.

Furthermore, we can replace $B(r_S)^2$ in equation 2.12 to include the stand-off distance r_S and the surface magnetic field strength B_0 on Mars using the dipole approximation (see equation 2.11). Therefore:

$$P_{ram} \cdot 2\mu_0 = B(r_S)^2 = {B_0}^2 \cdot \left(\frac{r_M}{r_S}\right)^6 \tag{2.17}$$

or:

$$B_0 = (P_{ram} \cdot 2\mu_0)^{\frac{1}{2}} \cdot \left(\frac{r_S}{r_M}\right)^3 \quad 2.18$$

where r_M is the radius of Mars (see [19]). Evaluating B_0 for maximum ram pressure (1.3 μPa from before) and for stand-off distance $r_S = 1.3r_M$ results in a surface magnetic field strength of 4.0 μT or 0.040 Gs, accordingly. Earth's magnetic field ranges from 24 μT to 66 μT (e.g. [21][22]). Surface intensity on Earth is therefore up to 17 times stronger than it would be on Mars. $1.3r_M$ is chosen for r_s to provide some buffer when protecting an artificial atmosphere.

DuPont and Murphy [15] do not justify their stand-off distance of $2r_M$. This paper will show by analogy to Earth that even $1.3r_M$ should suffice: Almost all our atmosphere is contained below the exosphere, the outermost atmospheric layer. The altitude of its lower boundary (the exobase) ranges from 500 km to 1000 km [23]. Next, we want to find equivalent altitudes for an artificial Martian atmosphere, which is necessary in a terraforming scenario. We will assume a scaled-down version of Earth's atmosphere. An exact analysis of how an artificial atmosphere for Mars should be composed and layered, however, lies beyond the scope of this paper.

The property which defines an exobase will here be simplified to the ratio of gravitational force on the surface versus at the exobase for any object with mass. In reality, one would have to account for other effects. Equating these ratios for Earth and Mars yields:

$$\frac{F_{S,E}}{F_{exo,E}} = \frac{F_{S,M}}{F_{exo,M}} \quad 2.19$$

with $F_{S,E}$ and $F_{S,M}$ being the gravitational force at the surface of Earth and Mars and $F_{exo,E}$ and $F_{exo,M}$ at the exobase. From Newton's law of gravitation, the left and right side reduce to:

$$\frac{r_{exo,E}^2}{r_E^2} = \frac{r_{exo,M}^2}{r_M^2} \quad 2.20$$

with $r_{exo,E}$ and $r_{exo,M}$ being the distances from the planets' centers to the exobase and r_M and r_E the radii. Rearranging equation 2.20:

$$r_{exo,M} = \frac{r_{exo,E}}{r_E} \cdot r_M \quad 2.21$$

$r_{exo,M}$ assumes $3.92 \cdot 10^6$ m given $r_{exo,E} = r_E + 1000$ km. This means an exobase altitude of ~530 km or $\sim 0.156r_M$ for Mars. Again, planetary radii are taken from [19]. It is prudent to at least double this value to account for any underestimations to $0.3R_M$, confirming a minimum stand-off distance of $1.3R_M$.

3 Methods

3.1 Restarting Mars's Dynamo

3.1.1 Dynamo Theory and Planetary Magnetic Fields

Earth generates its magnetic field by means of a dynamo effect. The general idea of the first method is to copy this mechanism to produce a magnetosphere for Mars.

Here is an outline of how the dynamo effect works on Earth: Earth's core is made up of a solid inner core with radius of 1221 km and a liquid outer core which extends to 3480 km [24]. Both are composed of iron, some nickel, and trace amounts of lighter elements [25]. The fluid in the outer core is in motion due to convection. Two types of convection power the geodynamo [25]: Compositional convection is driven by the buoyancy of lighter elements, which rise into the liquid outer core after exclusion from solidification together with the sinking iron at the inner core. Thermal convection is driven by temperature differences: Alfè et al. [24] estimate temperature at the core-mantle boundary (CMB) to ~4000 K and at the boundary between the inner and outer core to $5400 - 5700$ K. The sources of this abundant thermal energy in the core are left-over heat from the planet's formation, frictional heating from compositional convection, and latent heat release during solidification of liquid material at the inner core [25]. Estimates state that around 80% of power to the dynamo is provided by compositional convection and the remaining 20% by thermal buoyancy, though the error margins are large [25]. The Coriolis force also plays a key role in the fluid's motion as it organizes flow patterns into vertical helices [26]. The presence of a "seed" magnetic field now exerts a magnetic force (see equation 2.3) on the moving, conductive liquid, producing a current within. Equally, this current induces a new magnetic field due to Ampère's circuital law (equation 2.4), which again influences currents in the fluid. This process creates a feedback effect, and so, the resulting amplified magnetic field (see Figure 5) has to be modelled by non-linear partial differential equations, for which numerical solutions have become feasible only under idealized conditions [26].

Mars's core would lend itself to an active dynamo: Its radius is approximated to be 1830 ± 40 km [27], which is about half the radius of Earth's core. Most importantly, it is also composed of an iron-nickel alloy with trace amounts of lighter elements (S, C, Si, O, N, and H) [28]. Its sulfur content is much higher, though, with estimates thanks to meteorites whose parent body is Mars ranging from ~11% to 15% mass [29], while the maximum content in Earth's core is 1.7%, according to [30]. Models of the interior of Mars by Sohl and Spohn [31] suggest that central temperature is in the 2000 to 2200 K range and the temperature at the core-mantle boundary is around 1750 to 1900 K. There is uncertainty and lack of consensus regarding the existence of a solid, inner core similar to Earth's (e.g., [28, 32]) since little is known of Mars's planetary physics. New seismic data from NASA's InSight mission to Mars has confirmed a liquid component of Mars's core, but the presence of an inner core remains uncertain according to the authors [27].

Moreover, a dynamo for Mars might be a plausible idea because there is substantial evidence to indicate an ancient Martian dynamo. Locally strong crustal magnetic sources suggest an ancient magnetic field of interior origin [33]. This stands in contrast to the overall weak present field of at maximum ~0.5 nT or $5 \cdot 10^{-4}$ μT [4] (compare to our desired strength of at least 4.0 μT calculated in section 2.2). This raises the question why the Martian dynamo ceased to function. The three possibilities are [34]: Firstly,

and this is the most well-developed theory, core cooling rate decreased drastically because the core became too cold meaning that thermal energy loss from the core decreased. Additionally, compositional convection fails to occur because no inner core formed. So, neither thermal energy nor gravitational energy are being converted into magnetic energy. Secondly, convection patterns changed from an efficient mode like Earth's to a stagnant mode, which prevents efficient compositional convection and efficient core cooling. This explanation works for both the absence and presence of an inner core. Thirdly, Mars's inner core increased in size sufficiently to render the liquid core too thin to sustain a dynamo.

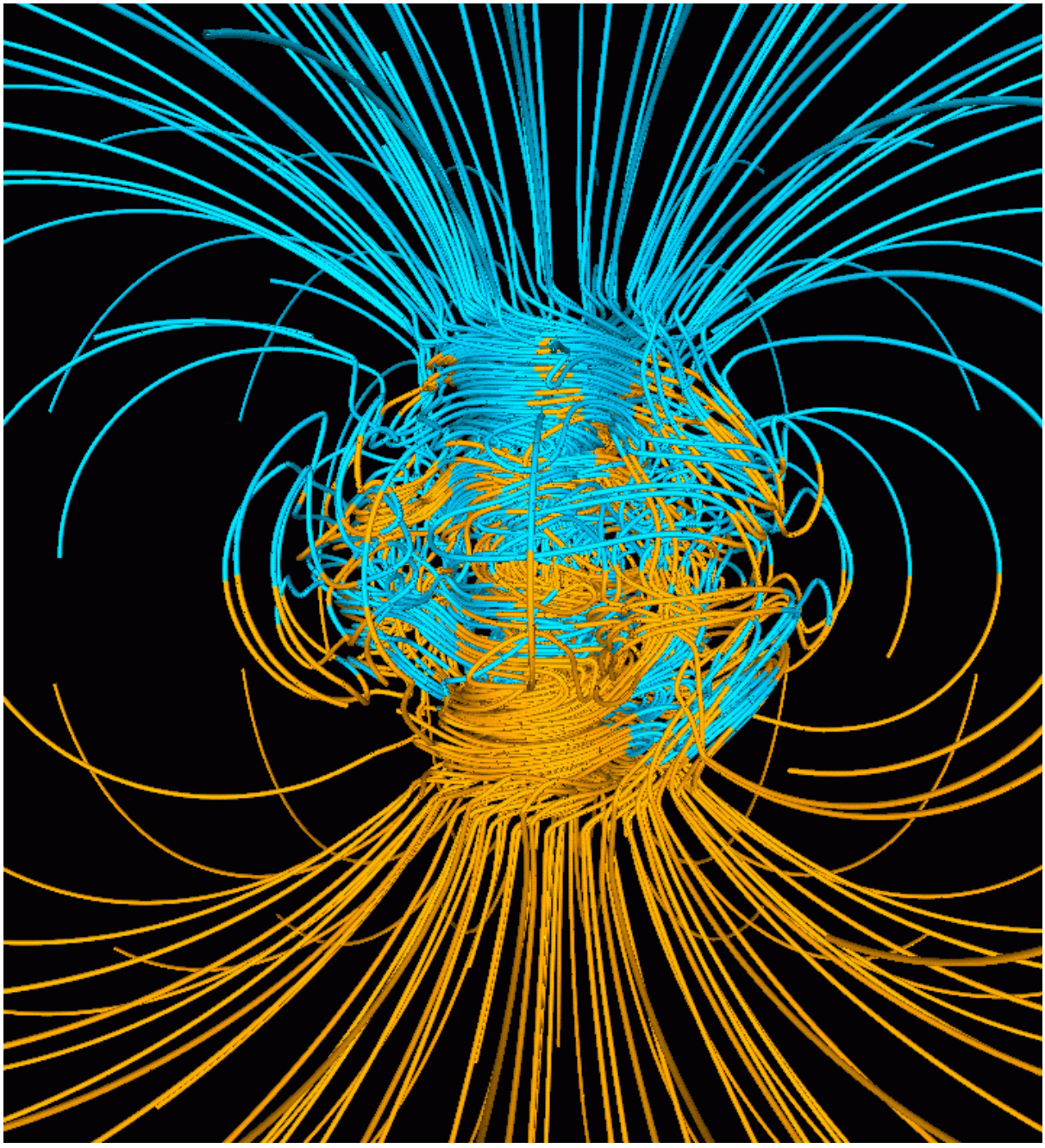

Figure 5: A snapshot of Earth's magnetic field simulated by the Glatzmaier-Roberts geodynamo model [35]. Field lines are yellow where the radial component is facing outward and blue where it is facing inward. The rotational axis is vertical. Outside the core, the field strongly resembles a magnetic dipole. Inside the core, the field is much more chaotic and intense.

3.1.2 Energy Requirements

Bamford et al. [36] propose heating Mars's core until it matches the temperature of Earth's in an effort to reinvigorate its lost dynamo. However, they do not differentiate between the different scenarios of the dynamo's death and arbitrarily state some goal temperature; we will account for these preconditions, and we will try to calculate some reasonable value. However, we will still make some simplifying assumptions because of the complexity of dynamo theory. First of all, the component of B powered by thermal convection, B_t, is roughly proportional to core heat loss rate $\dot{Q}$ because, as mentioned, energy that is lost from the core powers the dynamo. Furthermore, we assert intuitively that the ratio between $\dot{Q}$ and the conductive heat loss at the CMB $\frac{\dot{Q}}{\dot{Q}_{CMB}}$ is constant:

$$B_t \propto \dot{Q} \Leftrightarrow B_t = c\dot{Q} \Leftrightarrow B_t = k\dot{Q}_{CMB} \tag{3.1}$$

where c and k are some constants. Conductive heat transfer in a hollow sphere (synonymous to heat loss from the CMB to the planet surface: $\dot{Q}_{CMB}$) is described as follows:

$$\dot{Q}_{conductive} = \frac{T_1 - T_2}{r_2 - r_1} \cdot 4\pi r_1 r_2 \lambda \tag{3.2}$$

where r_1 is the inner radius, r_2 is the outer radius, T_1 and T_2 are the temperatures of the respective radii, and λ is the heat conductivity of the hollow sphere. The above equation can be derived from the one-dimensional version of Fourier's law [37] as conduction proceeds only radially when considering a sphere:

$$q = -\lambda \frac{dT}{dx} \tag{3.3}$$

Here, q is heat flux, which is measured in $\frac{\mathrm{W}}{\mathrm{m}^2}$, and $\frac{dT}{dx}$ is the temperature gradient.

Our second key assumption is that B_t is constant provided that the ratio between the core radius and the absolute distance from the planet's center is constant. Of course, heat loss rate also has to be constant as a precondition. In other words, scaling down the size of the dynamo will not have any effect on B_t as long as distance from the planet is also scaled down accordingly.

Combining equation 3.2 with our assumptions yields:

$$B_{t,\frac{r_C}{d}} = k \cdot \left(\frac{T_C - T_S}{r - r_C} \cdot 4\pi r_C r \lambda \right) \tag{3.4}$$

The left-hand side represents the thermal component of field strength at some *fixed ratio* $\frac{r_C}{d}$ between core radius r_C and distance from the center d. k is the constant from equation 3.1 assumed to be equal for Earth and Mars. T_C is the core temperature, T_S is surface temperature, and r is the planet radius. Heat conductivity of the mantle λ will be assumed to be equal for Earth and Mars as the true values, which actually vary with depth, lie in the same order of magnitude [38, 39, 40].

The ratio between core and planet radius is almost the same for Earth and Mars with $\frac{r_{C,E}}{r_E} \approx \frac{r_{C,M}}{r_M} \approx 0.5$ (see section 3.1.1 as well as [19]). Therefore, we will calculate the constant k for the ratio $\frac{r_C}{d} = 0.5$, using data from Earth. The constant $k_{0.5}$ will then pertain to surface magnetic field strength for both planets:

$$k_{0.5} = \frac{B_{t,E,0.5}(r_E - r_{C,E})}{(T_{C,E} - T_{S,E})4\pi r_{C,E} r_E \lambda} \tag{3.5}$$

In the first, most likely scenario of the death of Mars's magnetic field, an inner core did not form, so we cannot expect it to do so when we heat the core up. The dynamo will have to run solely on thermal convection, meaning $B_{t,M}$ at the surface, or synonymously $B_{t,M,0.5}$ will have to equal 4.0 µT (computed in section 2.2). Therefore, from equation 3.4 and using $k_{0.5}$ from equation 3.5:

$$B_{t,M,0.5} = \frac{B_{t,E,0.5}(r_E - r_{C,E})}{(T_{C,E} - T_{S,E}) \cdot 4\pi r_{C,E} r_E \lambda} \cdot \frac{T_{C,M} - T_{S,M}}{r_M - r_{C,M}} \cdot 4\pi r_{C,M} r_M \lambda \tag{3.6}$$

where quantities labeled with subscript E and M indicate their correspondence to Earth and Mars. Remember that $B_{t,M,0.5}$ and $B_{t,E,0.5}$ both concern surface intensity with the ratios between core radius and planetary radius being ~0.5. Additionally, the thermal component of magnetic field strength on Earth $B_{t,E,0.5}$ is 20% of total field strength, as discussed in section 3.1.1. A mid-range value for total intensity on Earth's surface is 45 µT [7, 8]. For $T_{C,E}$, a reasonable value of 5000 K (see section 3.1.1) can be used. Finally, average surface temperatures of 288 K for Earth and 208 K for Mars [41] are used. Solving 3.6 for $T_{C,M}$ yields:

$$T_{C,M} \approx \frac{B_{t,M,0.5}(T_{C,E} - T_{S,E})(r_M - r_{C,M}) r_{C,E} r_E}{0.2 B_{tot,E}(r_E - r_{C,E}) r_{C,M} r_M} + T_{S,M} \approx 4200 \text{ K} \tag{3.7}$$

Increasing the temperature of the Martian core from a mid-range value of 1960 K (see section 3.1.1) to ~4200 K requires the following amount of heat:

$$Q = c_{C,M} m_{C,M} \Delta T = \frac{4}{3} \pi r_{C,M}^3 \rho_{C,M} c_{C,M} \Delta T \approx 2.1 \cdot 10^{29} \text{ J} \tag{3.8}$$

where $c_{C,M}$ is specific heat capacity of the Martian core. We approximate this with 600 $\frac{\text{J}}{\text{kg·K}}$, which is characteristic for iron containing 11% sulfur by mass [28]. Mean core density of Mars $\rho_{C,M}$ is estimated to be 5.7 to 6.3 $\frac{\text{g}}{\text{cm}^3}$ [27], so we use the average of 6000 $\frac{\text{kg}}{\text{m}^3}$ in the above calculation. Of course, the result here does not include other issues such as drilling and heat loss, which may well raise energy requirements by another order of magnitude.

According to the International Energy Agency [42], global energy consumption in 2019 was $6.17 \cdot 10^{20}$ J. Heating the core would require at least 340 million times more than that. Another way to conceptualize $2.1 \cdot 10^{29}$ J is to calculate how many nuclear power plants would have to run during a period of, for example, one year. If we consider the net electrical power generation of Switzerland's most powerful nuclear reactor in Leibstadt with an output of 1220 MW [43], we will need at least 5.5 trillion of them.

Under the second hypothesis of the dynamo's death, we would have to invest the same amount of energy to restart it if, again, we were to approximate magnetic field strength to be proportional to core cooling rate. Plausibly, energy requirements would be lower in the case of the existence of an inner core because compositional convection would additionally power the dynamo. However, it is entirely conceivable that there is a much more energy-efficient way to change convection patterns from this stagnant back to a productive mode, which is hidden in the complexities of dynamo theory. A separate paper might like to investigate this issue. Under the third hypothesis, energy requirements would probably be of the same order of magnitude as the energy requirements posited by the first hypothesis; additional heating

is required for the phase transition, but the necessary core temperature is lower due to compositional convection contributing to the dynamo.

The most significant unresolved issue in all scenarios is the "seed" magnetic field, which is necessary for any dynamo to start functioning. Further research might endeavor to determine whether the strong local magnetization of the crust is sufficient for this purpose.

3.2 Plasma Torus

3.2.1 Infrastructure

Bamford et al. [36] further propose that one could construct a rotating ring of plasma (i.e. a torus, see Figure 6) around the planet. Since a plasma is essentially a pool of electrons, ions, and possibly neutral particles [44], this will constitute a current and therefore also a dipole-like magnetic field, analogous to the magnetic field of a current loop. We need infrastructure to maintain the bulk velocity, compensate thermal energy losses, and guide the trajectory of the charge-carriers. Three different torus positions are possible: on the surface with $R = r_M$, where the infrastructure would be very accessible. However, we

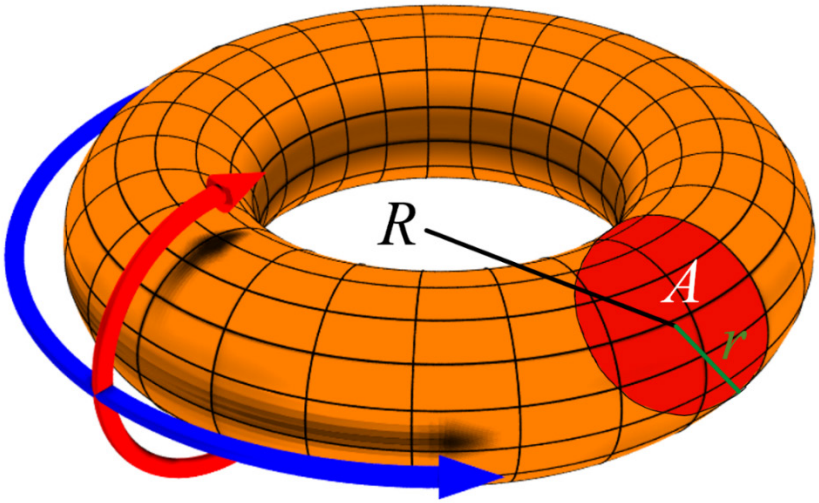

Figure 6: A torus. R is its major radius, r its minor radius, and A its cross-sectional area. The red arrow indicates the poloidal direction, and the blue arrow the toroidal direction.

will discard this idea because this would raise the infrastructure demands enormously; the confinement of the plasma would have to be near perfect to maintain surface habitability in the vicinity of the torus. Next, we could place a very compact torus at the L_1 point between the Sun and Mars (see Figure 8), where the gravitational attraction from the two bodies is in equilibrium, about a million kilometers from Mars's center of mass [45]. The problem with this approach is, on the one hand, the distance from the Martian surface, complicating construction and maintenance. On the other hand, protection from galactic cosmic rays, which come from all directions, is severely limited. Even the protection from solar radiation cannot be guaranteed as magnetotails are known to undulate under varying solar wind conditions (see [46] for an in-depth summary of the behavior of Earth's magnetotail). Bamford et al. [36]

solely propose the optimal solution of placing the torus in the orbit of a Martian moon, Phobos or Deimos, which would allow us to evaporate material off one of them to form the torus. Because the first exhibits larger dimensions than the second [47], the authors argue that the increased surface area would provide more evaporation capacity and space for the necessary infrastructure, such as nuclear power generators. One could add that the shorter mean distance of Phobos to Mars's surface ($1.77r_M$ versus $5.91r_M$ [47]) is also a significant advantage, facilitating maintenance work, as well as its mass, which is about ten times greater [47], extending the lifetime of the torus.

Valuable insights into plasma confinement have been produced by research into nuclear fusion power; tokamak devices, which are the most well-funded and understood approach, work by trapping the plasma in a torus shape by means of magnetic fields. In essence, a helical magnetic field around the plasma torus is required to keep it stable. This resultant field consists of a superposition of three magnetic fields (see Figure 7): one in the toroidal direction generated by multiple coils wrapped around the torus, another in the poloidal direction generated by the current inside the plasma, and a vertical third generated by coils about the toroidal field coils [48].

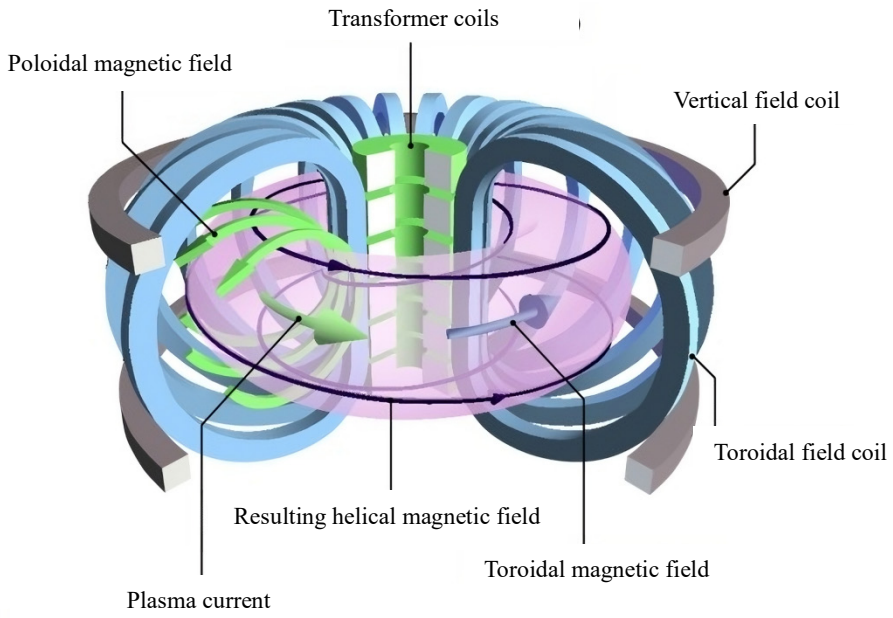

Figure 7: Structure of a tokamak. The transformer's function is to induce the plasma current.

We can directly compare the Martian torus to a scaled-up version of a tokamak like Bamford et al. [36]. This implies the necessity of current loops all around the orbit of Phobos, which are to impose a guiding magnetic field along the toroidal axis. However, this paper will add that we will likely have more leeway concerning the toroidal field coil density along the trajectory as particle losses are acceptable here in space as long as the ionization of Phobos can compensate for them. This is why a surface plasma torus would require that much more infrastructure. The poloidal component will be given by the plasma current. This paper will add that the vertical coils might be dispensable because their purpose in tokamaks is only to fix the plasma current in place. Such a fixation might even be counterproductive for the Martian torus as we want to maximize the current for a strong magnetic shield. This paper also argues that the implementation of a large enough transformer would be impractical. Besides, a transformer cannot generate a continuous current since it works in pulses [48], but we would like a continuous magnetic shield for Mars. Instead, a current-drive system could be used as proposed by Bamford et al. [36]. A current-drive is based on either inducing electromagnetic waves or neutral particles asymmetrically into the plasma in order to generate a continuous plasma current [49].

In conclusion, the necessary infrastructure consists of numerous space-based current loops encircling the plasma all around the planet, each needing a power supply. More infrastructure is required to continuously generate the plasma current. Finally, a way must be found to keep the plasma at an appropriate temperature by reheating it. To make these constructions more compact, they might be combined into singular space stations. A more detailed execution plan and concrete calculations, however, lie beyond the scope of this paper.

3.2.2 Energy Requirements

In the following, approximate energy requirements of the torus system itself, without accompanying logistics, will be investigated. First, we need to consider the total current I inside the structure:

$$I = \frac{Q_{tot}}{\Delta t} = Q_{tot}\frac{v}{\Delta s} = \frac{Q_{tot}}{A} A \cdot \frac{v}{\Delta s} = \frac{Q_{tot}}{V} Av = nq\pi r^2 v \tag{3.9}$$

where Q_{tot} is the total amount of charge passing through cross-sectional area A of the torus in a time frame Δt, v is bulk charge-carrier velocity assumed to be constant inside the torus, n the number density of the charge-carriers, and q is the charge of an individual particle. Here, we assumed uniform current density, drift velocity, and equal charge of the particles. Since a plasma contains both positive and negative charge carriers, we could give them opposite velocities to enhance the current, in which the above equation becomes:

$$I = \frac{Q_{tot,i}}{V} Av_i + \frac{Q_{tot,e}}{V} Av_e = (n_i v_i q_i + n_e v_e e)A \tag{3.10}$$

where n_i and n_e are ion and electron number densities, v_i and v_e their (positive) bulk velocities. q_i is ion charge and e is the elementary charge. One could further extend the equation to account for different ion charges. For simplicity's sake, however, we will only work with electrons. Bamford et al. [36] also show equations 3.9 and 3.10 but do not elaborate further.

We will assume that the magnetic field inside the plasma torus is uniform in regard to Mars. This is accurate enough as long as the torus radius R (here $2.77r_M$) is larger than r_M (see Figure 4 or equation 2.8). Combining equations 2.8 and 3.9 yields:

$$B_S = \frac{\mu_0 R^2}{2(R^2 + r_M^2)^{1.5}} I = \frac{\mu_0 R^2}{2(R^2 + r_M^2)^{1.5}} ne\pi r^2 v \tag{3.11}$$

We now want to solve for n. B_S has to be 4.0 µT as discussed in section 2.2. e is taken from [19]. We have chosen $x = r_M$ rather than $x < r_M$ (x is from equation 2.8) to get a conservative estimate. R is equal to $2.77r_M$ for our torus coinciding with the orbit of Phobos. A sensible minor radius could for example be twice the length of the major axis of Phobos, which results in 52 km [47]. This would allow enough space for the material being ionized from Phobos to be contained without excessive operational effort. However, we still want to keep the radius as small as possible to minimize the logistics of guiding and reheating the plasma. $v = 3.0 \cdot 10^6 \ \frac{\mathrm{m}}{\mathrm{s}}$ is derived on the next page.

$$n = \frac{2B_S(R^2 + r_M^2)^{1.5}}{\mu_0 R^2 e\pi r^2 v} \approx 1.8 \cdot 10^{10} \ \mathrm{m^{-3}} \tag{3.12}$$

The bulk velocity v of the electrons has to be high enough to reduce outward drift and a consequent loss of the charge-carriers; this is facilitated if it exceeds the thermal velocity of single electrons. To determine a possible *thermal* velocity, we examine the energy range of the natural space plasma around the Earth, which spans from 0.1 eV to 100 keV [50]. The following equation relates the kinetic energy to *thermal* velocity v_{th} without taking into account relativistic effects, which will be negligible for the energies we will work with:

$$\frac{1}{2}m_e v_{th}^2 = E_{kin} \Longrightarrow v_{th} = \sqrt{\frac{2E_{kin}}{m_e}} \tag{3.13}$$

We have to consider several factors when choosing an appropriate kinetic energy of a torus electron: on the one hand, kinetic energy has to be high enough in order to sustain the plasma state and keep ions and electrons separate. On the other, we want to keep energy requirements low. In addition, greater energies result in increased hazards for spacecraft passing through the torus; [50] suggests that electrons in the tens of keV to MeV range may penetrate the surface of the spacecraft and deposit charges inside, damaging vital electronic systems. This problem is even more pronounced when ions are included in the torus due to their greater mass. We will therefore choose an arbitrary kinetic energy of 1 eV, which is on the low end compared to the energy range of Earth's plasma. Of course, lower energies can, too, lead to problems such as surface charging [50], where potential differences on the spacecraft hull cause electric discharges, which may interfere with onboard electronics or directly damage spacecraft components. Mitigating these risks through clever engineering choices and material selection, however, is easier than stopping high-energy particles from penetrating the hull.

$1eV$ corresponds to a thermal velocity of $\sim 5.9 \cdot 10^5 \ \frac{\mathrm{m}}{\mathrm{s}}$ according to equation 3.13. As stated before, ideally, the bulk velocity would best far exceed it. However, considering the escalating difficulty of guiding a rapidly rotating plasma torus, we will limit the bulk velocity of the plasma equal to five times the thermal velocity.

With $n \approx 1.8 \cdot 10^{10}$ m^{-3} and $v_{th} \approx 5.9 \cdot 10^5 \ \frac{\mathrm{m}}{\mathrm{s}}$, the make-up of the torus closely resembles low-earth-orbit plasma conditions (high density, low energy) [50], with the exception of the bulk plasma movement $v = 5v_{th}$, indicating it would probably still be possible for spacecraft to pass through the torus, though avoiding longer stays, if possible, would be prudent.

Using the number density n, we can compute further relevant data on the torus; the total number of electrons has to be

$$nV = n \cdot 2\pi^2 r^2 R = 8.9 \cdot 10^{27} \tag{3.14}$$

from the volume of a torus. Since we defined the kinetic energy of a single electron before (1 eV), we can compute the total internal energy of the torus system: $1.4 \cdot 10^9$ J. The nuclear reactor in Leibstadt would have to run for only ~ 1.2 s to generate such an amount of energy. This value also provides information on the power requirements of maintaining plasma temperature as kinetic energy is lost all the time to thermal radiation, requiring constant replenishment; as an upper bound, one could dictate that the entire internal energy of the system is lost in a second, implying a maintenance power of $1.4 \cdot 10^9$ W. This is, of course, a very conservative estimate seeing that the system will most likely not cool to absolute zero in a second.

The kinetic energy stored in the bulk rotation of the torus sounds equally achievable:

$$E_{kin} = \frac{1}{2} m_{tot} v^2 = \frac{1}{2} n V m_e v^2 \approx 3.6 \cdot 10^{10}\ \text{J} \tag{3.15}$$

because we had assumed bulk velocity v was uniform; velocity in circular motion is angular velocity times distance from the center, and since $R \gg r$ for our planetary torus, the fluctuation of v is small compared to its total value. m_e is taken from [19]. In conclusion, what makes the plasma torus a futuristic scenario does not stem so much from the intrinsic energy requirements, but rather from the complex infrastructure.

3.3 Electromagnets

3.3.1 Superconductors

The idea is analogously to have a current generate a magnetic field which counters ram pressure from cosmic radiation. This time, the current would run inside multiple loops of wire, bundled together into a torus shape. The important quality of the wire is its *superconductivity*, which will briefly be discussed now, based on information adapted from [51]. Superconductivity is a property which is defined by the expulsion of magnetic field from within a material, termed the *Meissner effect*, and by zero electrical resistance. The absence of electrical resistance would theoretically allow a direct current to flow eternally without diminishing and without requiring any voltage. Consequently, because no power is lost, the wire does not heat up. We can use these traits to try to minimize energy requirements for the Martian shield. Superconductivity has been reported in about 30 elements and several thousand metallic alloys and chemical compounds. The caveat is that only below a critical magnetic field B_c at the conductor's surface and only below a specific transition temperature T_c do these materials demonstrate superconductivity. For many materials, T_c is below 77 K, requiring the use of expensive liquid helium for cooling. More recently discovered materials exhibit a higher T_c which is still well below room temperature but allows for cooling with the much more affordable liquid nitrogen. These high-temperature superconductors (HTS) also have a higher B_c. Owing to these advancements, many applications have become more economically viable. Often, however, HTS are characterized by challenging mechanical properties such as brittleness.

Returning to the Martian magnetosphere, DuPont and Murphy [15] derive a relation for relevant parameters:

$$V_S \approx 128 \frac{B(r_s)^2 r_M^6}{B_o^2 a^3} \tag{3.16}$$

where V_S is the volume and a is the major radius of the superconductor. $B(r_s)$ is the magnetic field at a desired stand-off distance, which ought to be $B(1.3r_M) = 1.8$ µT, as demonstrated in section 2.2. B_o is the magnetic field at the surface of the operating superconductor, meaning it must be less than the material-specific critical magnetic field B_c. The relevant idea this equation conveys is that the necessary volume of the superconductor is inversely proportional to the square of B_o and the cube of a.

DuPont and Murphy [15] further suggest three possible materials for the Martian superconductor: carbon nanotubes, yttrium barium copper oxide (YBCO), and bismuth strontium calcium copper oxides (BSCCO). The advantage of carbon nanotubes is, of course, the abundancy of carbon in nature and their extensively studied synthesis, which is easy to scale up, with large quantities (10 to 100 g per day)

already being produced in some laboratories [52]. However, we will have to discard carbon nanotubes due to contentions concerning their superconductivity [53] and reported T_c being very low ($\sim$15 K) in studies that identify a resistivity drop [54, 55]. Ideally, the superconductor should operate at temperatures as high as possible in order to minimize the engineering challenges of achieving and maintaining the superconducting state below T_c on a planetary scale.

In contrast, YBCO and BSCCO are classified as high temperature superconductors with critical temperatures of 80 K [56] and up to 108 K [57], respectively. Additionally, their critical fields are also very high at 168 ± 28 T for YBCO and up to 200 ± 25 T for BSCCO, both measured at 4.2 K [58]. It is relevant to note that B_c is temperature-dependent and decreases to zero as temperature approaches T_c for all superconductors [59], which [15] does not take into account. Moreover, the space for most applications of high-temperature superconductors lies below the smaller irreversibility field $B_{irr}(T)$ instead of the larger $B_c(T)$, because in the range between these two, certain magnetic effects inhibit lossless current flow despite the material still being in a superconducting state according to quantum mechanical considerations [60]. It turns out that despite BSCCO's higher critical field and higher transition temperature, YBCO is starting to replace it in most applications due to its higher irreversibility field [61], which allows for the generation of stronger magnetic fields: the new second generation HTS wires, based on coated conductor technology, prefer the use of YBCO and additionally exhibit superior mechanical properties to the first generation wires [62], which use BSCCO. Manufacture of the 2G wires is already proceeding in kilometer lengths [62].

We will therefore choose to construct the Martian superconductor with YBCO and now try to minimize the necessary volume given by equation 3.16. An operational temperature of 50 K seems reasonable, allowing the superconductor to work at 30 T [63]. Significantly lower temperatures would be hard to maintain from an engineering standpoint, and temperatures closer to T_c would drastically lower B_{irr} and subsequently increase the volume. A suitable major radius a could be r_M since that would allow wrapping the superconductor around the planet, while loops of larger radius would necessitate placement in orbit, complicating the engineering of the cooling infrastructure, so they are not worth the decrease in superconductor volume. Concretely, these values imply a necessary volume of $1.8 \cdot 10^7$ m^3 according to equation 3.16. From the volume of a torus, the minor radius of the superconducting wire bundle is computed to 0.5 m. The superconductor's mass is $1.1 \cdot 10^{11}$ kg assuming a maximal density of YBCO, 6370 $\frac{\text{kg}}{\text{m}^3}$ [64]. Notice that these results do not include other materials required in YBCO wires.

We can now estimate the bulk amount of rock required to extract the elemental ingredients of the necessary YBCO. The assumption is the mining of Earth's continental crust, to which access is the easiest. This means Yttrium will be the rarest element to gather, and it will therefore dictate the mass of the continental crust required. Yttrium's total mass in our superconductor is $1.8 \cdot 10^{10}$ kg supposing a realistic relation $Y{:}\,2Ba{:}\,3Cu{:}\,7O$ between the elements [56]. Abundance of Yttrium in Earth's crust is about $3.3 \cdot 10^{-3}$% by mass [65]. Earth's continental crust constitutes 0.40% [66] of its total mass (see [19]) and consequently has a mass of $2.4 \cdot 10^{22}$ kg, in which $7.9 \cdot 10^{17}$ kg of Yttrium are contained. Dividing the necessary Yttrium by this number and assuming a more realistic yield of 50% instead of 100% reveals that $4.4 \cdot 10^{-6}$% of Earth's continental crust would have to be mined. This is certainly a feasible undertaking, especially if the mining is complemented on Mars or on asteroids.

Equation 3.16 also showcases that a compact superconducting torus of a 20 km major radius, for example, falls short, as volume increases by a factor of $\sim$28720. Like in section 3.2.1, the idea would have been to place the object at the L_1 point about one million kilometers away from Mars (see Figure

8), instead of placing the torus around Mars's center. This would be possible because maximum ram pressure from the solar wind is not much larger at the L_1 point than near the planet, given its much greater distance from the Sun, around 227 million kilometers [45]. The dipole's magnetic field would therefore still be able to deflect the charged particles from the Sun. As discussed before, further problems include distance of the superconductor from the Martian surface, which complicates construction and maintenance, severely limited protection from galactic cosmic rays, which come from all directions, and magnetotails known to undulate under varying solar wind conditions (see [46]). Inspecting the effectiveness of a magnetic shield at the L_1 point in detail is beyond the scope of this analysis. For now, we can discard even superconductors of large major radius placed at the L_1 point due to these problems.

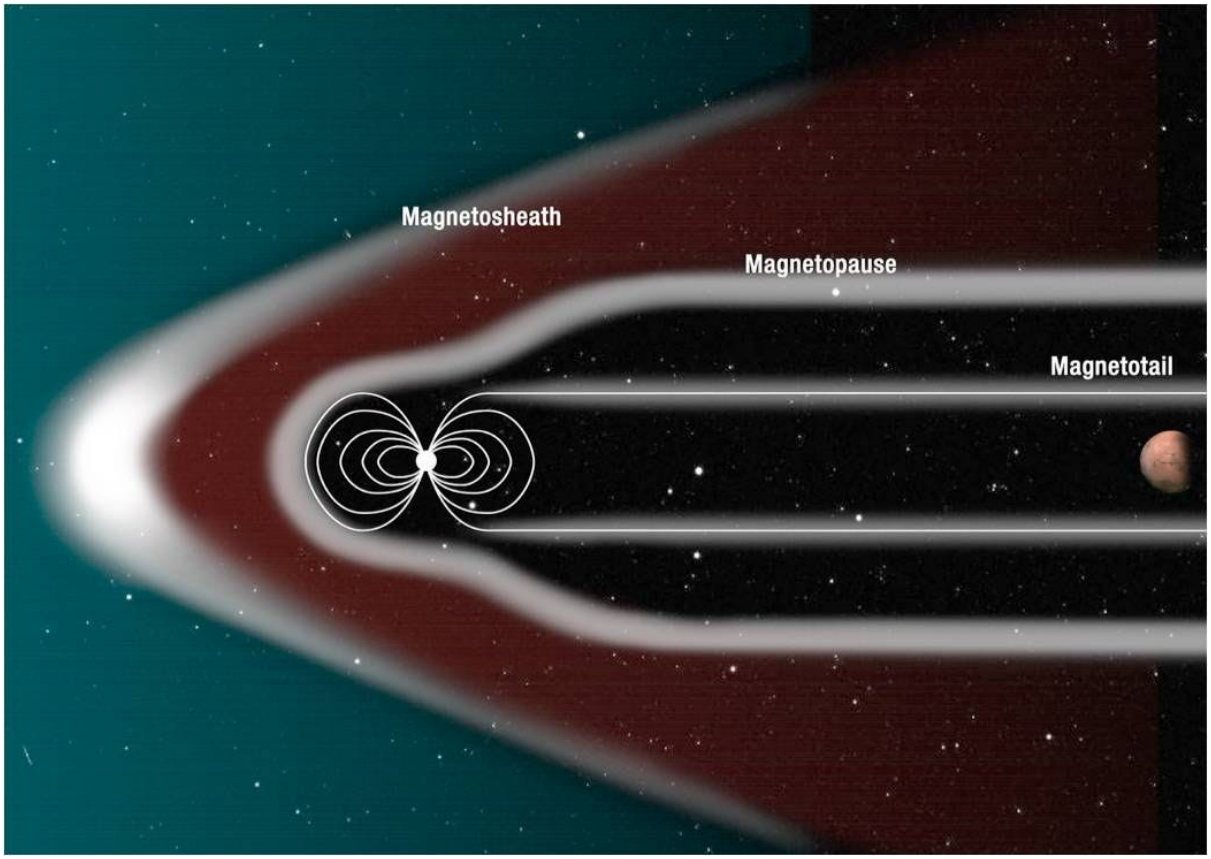

Figure 8: An electromagnet or plasma torus at the L_1 point in the Sun-Mars system. The magnetosheath marks where particles are influenced by the magnetic field. The magnetopause indicates where most particles are deflected.

An indicator regarding energy requirements to cool our superconductor of radius r_M is heat conduction. We will wrap the YBCO in a layer made of vacuum-insulated panels, as proposed by DuPont and Murphy [15], with heat conductivity as low as $0.004\ \frac{\mathrm{W}}{\mathrm{m \cdot K}}$. For the purpose of this calculation, the radius of the tube consisting of the superconductor and the insulator will consistently be 1 m. Conductive heat transfer in the insulator is described analogously to heat transfer of a hollow cylinder since the tube is essentially just a cylinder curved around the planet:

$$\dot{Q} = \frac{T_1 - T_2}{\ln\left(\frac{r_2}{r_1}\right)} \cdot 2\pi L\lambda = -0.18\ \mathrm{GW} \tag{3.17}$$

where r_1 is the inner radius, r_2 is the outer radius, T_1 and T_2 are the temperatures of the respective radii, λ is the heat conductivity, and L is cylinder length. DuPont and Murphy [15] use a different approach.

As a reminder, T_1 is 50 K, L is the circumference of Mars, and we will take T_2 to be the average surface temperature on Earth, namely 288 K; the terraforming of Mars also encompasses achieving this temperature. The negative sign shows that the heat flows towards the superconductor. The cooling system's task is to remove 0.18 GW of power in order to keep the internal energy constant. Since no cooling system is one-hundred percent efficient, though, the energy requirements might potentially be higher by up to an order of magnitude. Even so, the power involved is entirely attainable, showing that the challenge lies predominantly in manufacturing the superconductor and building the cooling infrastructure.

As a side note, the above equation could again be derived from the one-dimensional version of Fourier's law [37].

3.3.2 Conventional Conductors

The advantages of conventional conductors are that they do not require elaborate cooling infrastructure and that manufacture is easier and more cost-effective. A sensible material choice for our project might be copper, which is very commonly used in cables due to its low resistivity, $1.754 \cdot 10^{-8}$ Ωm at 20°C [19], and its cheapness; to illustrate, on the 27th of November 2023, the London Metal Exchange closed with a copper cash-settlement of 8281 US dollars per ton [67]. We will now estimate power demands of sustaining a large enough current in a copper wire loop based on the following equation:

$$P = UI = I^2 R_{el} \tag{3.18}$$

where P is the power the wire generates, U is voltage and R_{el} is the electrical resistance. Consequently, P is also the power which needs to be reintroduced into the wire. First, I is substituted with more relevant parameters according to equation 2.8:

$$P = \left(\frac{2B_0(\mathrm{R}^2 + r_M^2)^{1.5}}{\mu_0 \mathrm{R}^2} \right)^2 R_{el} \tag{3.19}$$

where B_0 is the desired surface field strength (4.0 μT), R the major radius of the loop, and r_M the radius of Mars. Notice that B_0 describes magnetic field strength only on the *axis* of the loop and at distance r_M, namely at the two points where the axis and the surface intersect. This is sufficient for the purpose of this estimation since the dipole's field would vary only moderately on the surface (compare to Earth, where it ranges only from 24 μT to 66 μT, e.g. [21] [22], or see Figure 4). Now R_{el} is substituted:

$$P = \frac{4B_0^2(\mathrm{R}^2 + r_M^2)^3}{\mu_0^2 \mathrm{R}^4} \rho_{\mathrm{el}} \frac{l}{A} = \frac{4B_0^2(\mathrm{R}^2 + r_M^2)^3}{\mu_0^2 \mathrm{R}^4} \rho_{\mathrm{el}} \frac{2\pi R}{\pi r^2} \tag{3.20}$$

$$= \frac{8B_0^2(\mathrm{R}^2 + r_M^2)^3}{\mu_0^2 \mathrm{R}^3 r^2} \rho_{\mathrm{el}} \tag{3.21}$$

$$= \frac{16\pi^2 B_0^2(\mathrm{R}^2 + r_M^2)^3}{\mu_0^2 \mathrm{R}^2 V} \rho_{\mathrm{el}} \tag{3.22}$$

where ρ_{el} is the material-specific electrical resistivity, here of copper, l the length of the wire, A its cross-sectional area, and r its minor radius. The final step replaces r^2 using the volume V of the toroidal wire. To show some concrete values, we will compute P for R equal to r_M, which would again allow us to encompass the diameter of Mars with the wire, as well as R equal to an arbitrary 20 km. In the latter case, the L_1 point is the most reasonable position but poses the same problems as discussed in section

3.3.1. Then, to reduce power, r in equation 3.21 or V in equation 3.22 should be as large as possible since they only occur in the denominator. The drawback is, of course, that increasing these values requires more copper. The first scenario is therefore $R = r_M$ and, arbitrarily, $r = 0.5$ m, mimicking the dimensions of the superconductor from before, which yields 1.8 PW, which is ~91 times more than the average global power consumption in 2019 [42]. The required volume is $1.7 \cdot 10^7$ m^3. The second scenario is $R = 20$ km and $r = 6.509$ m, resulting in the same volume, and yields 6.4 EW, around $330'000$ times the average global power consumption in 2019 [42]. Using the volume of $1.7 \cdot 10^7$ m^3, the density of copper from [19], and its price on November 27th, we arrive at a total cost of ~1.2 trillion US dollars. This is only ~4.8% of the 2022 GDP of the USA (for the November 2023 dollar value) [68]. $2.1 \cdot 10^{-5}$% of the Earth's crust would have to be mined given an abundance of 60 µg·g^{-1} [65] and a 50% yield. This is somewhat more than was necessary for the Yttrium, but on the one hand, YBCO is made up other elements, which have to be mined, and on the other, it is practically a smaller challenge because copper extraction infrastructure is much better developed (in 2016, $19'400'000$ tons of copper and $6'000$ tons of Yttrium were produced [65]). However, we should still be cautious about increasing r in order to reduce power consumption because the copper will have to be expensively shipped from Earth if extraction on Mars is not well-established. Additionally, copper contents of the Martian mantle are estimated to only 2.0 ± 0.4 µg·g^{-1} [69].

It is now interesting to rephrase equation 3.22 as a function and analyze its properties:

$$P(R,V) = \frac{16\pi^2 B_0^2 (\mathrm{R}^2 + r_M^2)^3}{\mu_0^2 \mathrm{R}^2 V} \rho_{\mathrm{el}} \tag{3.23}$$

The inverse proportionality on volume is immediately obvious. For extreme values of R, the power requirements behave in the following way:

$$\lim_{R \to 0} P(R,V) = \infty \tag{3.24}$$

$$\lim_{R \to \infty} P(R,V) = \infty \tag{3.25}$$

This implies that local minima exist. Taking the derivative with respect to R and setting to it zero shows:

$$\frac{\partial}{\partial R} P(R,V) = 0 \;\Leftrightarrow\; R = \frac{r_M}{\sqrt{2}} \tag{3.26}$$

The exact mathematical steps are irrelevant for this paper and are left out for conciseness but could easily be retraced. The equations in 3.26 say that given some V, the least power is required if R is uniquely $\frac{r_M}{\sqrt{2}}$ or ~71% the radius of Mars. This also clarifies why power requirements were much greater for $R = 20$ km than for $R = r_M$.

Let us finally compute $P(\frac{r_M}{\sqrt{2}}, 1.7 \cdot 10^7 \text{ m}^3)$ for comparison: 1.5 PW or ~76 times the average global power consumption in 2019 [42], and r would be 0.59 m. For $P(\frac{r_M}{\sqrt{2}}, 76 \cdot 5.3 \cdot 10^6 \text{ m}^3)$, of course, we get the average global power consumption, but at 76 times the cost, that is 360% of the 2022 United States GDP, or all of the copper in $1.6 \cdot 10^{-3}$% of Earth's crust given 50% mining yield.

4 Feasibility and Applications to Current Space Travel

To conclude, we will discuss the feasibility of providing a planetary magnetic field to Mars and compare the methods. Restarting Mars's core is the most unrealistic. The challenge lies not only in the enormous amount of energy required but also in transferring it to the core, i.e. drilling kilometers deep into the planet to detonate bombs, for example. Then, energy leakages and losses will occur during the heating process, further raising energy requirements. At present, we cannot be certain that the dynamo would work at all: firstly, the local magnetization of the Martian crust might not suffice as a "seed" magnetic field, and we would additionally have to construct one. Next, the interior structure of Mars is not well understood; notably, the existence of a solid inner core remains uncertain. Finally, dynamos are very complex systems due to their chaotic, nonlinear behavior. Given these various scientific and engineering challenges and uncertainties, the prospect of restarting the Martian dynamo remains highly speculative.

The plasma torus circumvents these absurd energy requirements but comes with its own unique engineering hurdles. Although we have experience in plasma containment, drawing from progress in nuclear fusion technology, the scale of establishing and sustaining a plasma torus around Mars is not to be underestimated. Before a more comprehensive analysis of these hurdles is conducted, it is wrong to call this the most feasible method.

Conversely, electromagnets are more straight-forward concerning engineering hurdles. Superconductors require cooling infrastructure and thermal insulation, whereas conventional conductors are simpler, requiring only a source of voltage and maybe some cheap electrical insulation. Additionally, conventional conductors are more easily produced; copper, for example, is cheap and easy to extract. Superconductors, however, are often very complex compounds, cumbersome to produce and difficult to work with. Simpler materials, such as aluminum, only exhibit superconductivity at extremely low temperatures [70]. In exchange, the power needs of the conventional conductors are significant but still not nearly as futuristic as the energy needs to restart the dynamo. This obstacle might even diminish as humanity finds innovative ways to generate power, particularly in light of rapid advancements in nuclear fusion. Given the current state of technology, however, superconductors present are a more feasible approach to generating a magnetic shield for Mars. Furthermore, they have great potential for improvement concerning transition temperatures, critical magnetic fields, mechanical properties, etc. due to very active research in the field ([55], [70], and many others).

The insights of this paper might prove useful to space travel in the near future. Currently, human presence in space is limited to low Earth orbit (LEO) in the ISS, where the geomagnetic field still provides ample protection from radiation. The need for additional shielding besides the materials present for other uses (spacecraft structure and contents, water tanks, etc.) is low; NASA standards restrict occupational radiation exposure throughout an astronaut's career to a less than 3% increase in late cancer mortality probability [71]. The absolute radiation doses are then age and gender specific. Evidently, these standards are quite strict, but they are still effectively adhered to in LEO. However, studies such as [71] show that further reducing radiation exposure in LEO is plausible using shielding made from polyethylene, a cheap and stable material. In contrast, trying to achieve shielding using electromagnets like the ones for Mars would be absurd in this case. The cost of construction and maintenance far outweighs the slight health advantage to astronauts on the ISS. Nevertheless, this type of shielding might become interesting for extended space flights outside of Earth's magnetic field and atmosphere where mitigating radiation requires increasingly thicker shielding meaning more mass to carry in the spacecraft. The optimal solution might involve a hybrid of a physical and a magnetic shield, especially considering the possible advent of superconductors. This remains to be seen in more detailed future research.

5 Conclusion

When terraforming Mars, radiation from space proves a significant problem due to long-term hazards to human, animal, and plant biology. Cosmic rays would also dissipate any artificial atmosphere on Mars. This paper discusses three approaches to establish a planetary magnetic field around Mars in order to protect the planet from cosmic radiation: restarting Mars's dynamo, a plasma torus around Mars, and electromagnets. Given the current state of technology and scientific research, superconducting electromagnets seem to be the most reasonable approach. To arrive at this conclusion, this paper demonstrates order of magnitude calculations for energy requirements and logistical arguments. The main methodological shortcoming of this paper is the simplification of the calculations for conciseness. Nevertheless, the insights on feasibility in section 4 remain valid; indeed, the temperature of 4100 K from section 3.1.2 is only an extremely rough estimate due to the neglected complexity of dynamo theory, but it adequately shows that some more or less large temperature increase is necessary. This inevitably translates into exorbitant energy requirements due to the sheer mass of iron that needs to be heated. The accuracy of the calculations in section 3.2.2 are also limited because we neglected the intricacies of plasma physics, but even if we had included them, the intrinsic energy requirements of the torus would most likely stay low, so that the argument remains that the logistics and infrastructure pose the main challenge. The results in section 3.3.1 are probably the most accurate because we used the least simplifying assumptions. Additionally, the accurate and conservative 4.0 μT necessary on the surface of Mars (section 2.2) provides a buffer against underestimations in later chapters.

This paper has covered the most promising methods for building an artificial magnetosphere for Mars. Further research in connection with this topic should mainly elaborate on the infrastructure of a plasma torus or the detailed application of electromagnets.

Finally, we can say that building a magnetic field that spans an entire planet, be it even as close as Mars, will be a multigenerational project for the foreseeable future, which will demand significant energy and financial expenses. However, this would not be the only among humanity's notable achievements, from the construction of the pyramids and the Manhattan Project to landing on the Moon.

Acknowledgements

I would like to thank my supervisor Magnus Gienal for valuable tips and feedback.

Bibliography

[1] "Mars", in: NASA, last edited: 26.9.2023, https://www.nasa.gov/humans-in-space/humans-to-mars/ (accessed 17.11.2023)

[2] TED, "Elon Musk: A future worth getting excited about | TED | Tesla Texas Gigafactory interview", in: YouTube, 18.4.2023, https://www.youtube.com/watch?v=YRvf00NooN8 (accessed 17.11.23)

[3] P. Birch, "Terraforming Mars quickly", *Journal of British Interplanetary Society* **1992**, *45*(8), p. 331–340

[4] M. Acuña et al., "Magnetic field of Mars: Summary of results from the aerobraking and mapping orbits", *Journal of Geophysical Research* **2001**, *106*(10), p. 23403–23417, doi:10.1029/2000JE001404.

[5] L. Strigari, S. Strolin, A.G. Morganti, A. Bartoloni, "Dose-Effects Models for Space Radiobiology: An Overview on Dose-Effect Relationships", *Front Public Health* **2021**, *9*, 733337, doi:10.3389/fpubh.2021.733337

[6] J.C. Chancellor, G.B. Scott, J.P. Sutton, "Space Radiation: The Number One Risk to Astronaut Health beyond Low Earth Orbit", *Life* **2014**, *4*(3), p. 491–510, doi:10.3390/life4030491

[7] S. McKenna-Lawlor, P. Gonçalves, A. Keating, G. Reitz, D. Matthiä, "Overview of energetic particle hazards during prospective manned missions to Mars", *Planetary and Space Science* **2012**, *64*, p. 123–132, doi:10.1016/j.pss.2011.06.017.

[8] T.A. Mousseau, A.P. Møller, "Plants in the Light of Ionizing Radiation: What Have We Learned From Chernobyl, Fukushima, and Other "Hot" Places?", *Frontiers in Plant Science* **2020**, *11*, 552, doi:10.3389/fpls.2020.00552

[9] F. Leblanc, A. Martinez, J.Y. Chaufray, R. Modolo, T. Hara, J. Luhmann et al., "On Mars's atmospheric sputtering after MAVEN's first Martian year of measurements", *Geophysical Research Letters* **2018**, *45*, p. 4685–4691, doi:10.1002/2018GL077199

[10] D.M. Kass, Y.L. Yung, "Loss of Atmosphere from Mars Due to Solar Wind-Induced Sputtering", *Science* **1995**, *268*, p. 697–699, doi:10.1126/science.7732377

[11] G.R. North, *Encyclopedia of Atmospheric Sciences*, 2nd Edition, Elsevier, Amsterdam, **2015**, p. 168–177, doi:10.1016/B978-0-12-382225-3.00312-1

[12] P.P. Urone, R. Hinrichs, K. Dirks, M. Sharma, *College Physics*, OpenStax, Houston, Tex., **2020**, p. 935–1073

[13] D.C. Giancoli, *Physik: Lehr- und Übungsbuch*, 3rd Extended Edition, Pearson Deutschland, Munich, **2010**, p. 917–1010

[14] D. Newell, E. Tiesinga, "The International System of Units (SI)", 2019 Edition, Special Publication (NIST SP), National Institute of Standards and Technology, Gaithersburg, Md., p. 8–9, doi:10.6028/NIST.SP.330-2019

[15] M. DuPont, J. Murphy, "Fundamental physical and resource requirements for a Martian magnetic shield", *International Journal of Astrobiology* **2021**, *20*(3), p. 215–222, doi:10.1017/S1473550421000069.

[16] J.-H. Shue et al., "Magnetopause location under extreme solar wind conditions", *Journal of Geophysical Research* **1998**, *103*(A8), p. 17691–17700, doi:10.1029/98JA01103

[17] P. Odert, M. Leitzinger, A. Hanslmeier, H. Lammer, "Stellar coronal mass ejections – I. Estimating occurrence frequencies and mass-loss rates", *Monthly Notices of the Royal Astronomical Society* **2017**, *472*(1), p. 876–890, doi:10.1093/mnras/stx1969

[18] Ryuho Kataoka, *Extreme Space Weather*, 2022 Edition, Elsevier, San Diego, Calif., **2022**, p. 31–64

[19] Swiss-German Mathematics and Physics Commission, "Fundamentum Mathematik und Physik: Formeln, Begriffe, Tabellen für die Sekundarstufen I und II", 10th Edition, Orell Füssli Publishing, Zurich, **2019**, p. 101–124

[20] H.A. Elliott, C.J. Henney, D.J. McComas, C.W. Smith, B.J. Vasquez, "Temporal and radial variation of the solar wind temperature-speed relationship", *Journal of Geophysical Research* **2012**, *117*, A09102, doi:10.1029/2011JA017125.

[21] P. Alken, E. Thébault, C.D. Beggan et al., "International Geomagnetic Reference Field: the thirteenth generation", *Earth Planets Space* **2021**, *73*, 49, doi:10.1186/s40623-020-01288-x

[22] E. Thébault, C.C. Finlay, C.D. Beggan et al., "International Geomagnetic Reference Field: the 12th generation", *Earth Planet Space* **2015**, *67*, 79, doi:10.1186/s40623-015-0228-9

[23] "The Exosphere", in: UCAR: Center for Science Education, no date, https://scied.ucar.edu/learning-zone/atmosphere/exosphere (accessed 3.10.2023)

[24] D. Alfè, M.J. Gillan, G.D. Price, "Temperature and composition of the Earth's core", *Contemporary Physics* **2007**, *48*(2), p. 63–80, doi:10.1080/00107510701529653

[25] B.A. Buffet, "Earth's Core and the Geodynamo", **2000**, *Science 288*, p. 2007–2012, doi:10.1126/science.288.5473.2007

[26] N. Weiss, "Dynamos in planets, stars and galaxies" **2002**, *Astronomy & Geophysics*, *43*(3), p. 3.9–3.14, doi:10.1046/j.1468-4004.2002.43309.x

[27] S.C. Stähler, et al., "Seismic detection of the martian core", **2021**, *Science*, *373*(6553), p. 443–448 doi:10.1126/science.abi7730

[28] G. Helffrich, "Mars core structure—concise review and anticipated insights from InSight", *Progress in Earth and Planetary Science* **2017**, *4*, 24, doi:10.1186/s40645-017-0139-4

[29] K. Lodders, B. Fegley, "An Oxygen Isotope Model for the Composition of Mars", *Icarus* **1997**, *126*(2), p. 373–394, doi:10.1006/icar.1996.5653

[30] G. Dreibus, H. Palme, “Cosmochemical constraints on the sulfur content in the Earth's core”, *Geochimica et Cosmochimica Acta* **1996**, *60*(7), p. 1125–1130 doi:10.1016/0016-7037(96)00028-2

[31] F. Sohl, T. Spohn, “The interior structure of Mars: Implications from SNC meteorites”, *Journal of Geophysical Research* **1997**, *102*(1), p. 1613–1635, doi:10.1029/96JE03419

[32] A. Rivoldini, T.V. Hoolst, O. Verhoeven, A. Mocquet, V. Dehant, “Geodesy constraints on the interior structure and composition of Mars”, *Icarus* **2011**, *213*(2), p. 451–472, doi:10.1016/j.icarus.2011.03.024.

[33] J. Connerney, M. Acuña, N. Ness, et al., “Mars Crustal Magnetism”, *Space Science Reviews* **2004**, *111*, p. 1–32, doi:10.1023/B:SPAC.0000032719.40094.1d

[34] D.J. Stevenson, “Planetary magnetic fields”, *Earth and Planetary Science Letters* **2003**, *208*(1/2), p. 1–11, doi:10.1016/S0012-821X(02)01126-3

[35] G. Glatzmaiers, P. Roberts, “A three-dimensional self-consistent computer simulation of a geomagnetic field reversal” **1995**, *Nature 377*, p. 203–209, doi:10.1038/377203a0

[36] R.A. Bamford, B.J. Kellett, J.L. Green, C. Dong, V. Airapetian, R. Bingham, “How to create an artificial magnetosphere for Mars”, *Acta Astronautica* **2022**, *190*, p. 323–333, doi:10.1016/j.actaastro.2021.09.023.

[37] John H. Lienard IV, John H. Lienard V, *A Heat Transfer Textbook*, 3rd Edition, Phlogiston Press, Cambridge Mass., **2008**, p. 12–20

[38] F.D. Stacey, *Encyclopedia of Geomagnetism and Paleomagnetism*, 1st Edition, Springer, Dordrecht, **2007**, p. 688–689, doi.org/10.1007/978-1-4020-4423-6_213

[39] M.M. Geeth, N. Koker, D.J. Frost, C.A. McCammon, “Lattice thermal conductivity of lower mantle minerals and heat flux from Earth’s core”, Proceedings of the National Academy of Sciences **2011**, *108*(44), p. 17901–17904, doi:10.1073/pnas.1110594108

[40] S. Schumacher, D. Breuer, Correction to “Influence of a variable thermal conductivity on the thermochemical evolution of Mars”, *Journal of Geophysical Research* **2006**, *111*, E09011, doi:10.1029/2006JE002755.

[41] “Solar System Temperatures”, in: NASA Science, last edited: 15.10.2023, https://science.nasa.gov/resource/solar-system-temperatures/ (accessed 29.10.2023)

[42] “World Energy Balances: Overview”, in: IEA, **2021**, https://www.iea.org/reports/world-energy-balances-overview (accessed 1.11.2023)

[43] “Kernkraftwerk Leibstadt”, in: ENSI, no date, https://www.ensi.ch/de/themen/kkw-leibstadt/ (accessed 1.11.23)

[44] R. Sentis, “Mathematical Models and Methods for Plasma Physics, Volume 1 : Fluid Models”, 1st edition, Springer International Publishing, Cham, **2014**, p. 1–3

[45] “Lagrange Point”, in: Wikipeida, last edited: 11.11.2023, https://en.wikipedia.org/w/index.php?title=Lagrange_point&oldid=1184606465 (accessed 25.11.2023)

[46] A. Nishida, “The Earth's Dynamic Magnetotail”, *Space Science Reviews* **2000**, *91*, p. 507–577, doi:10.1023/A:1005223124330

[47] "Martian Moons", in: NASA Science, no date, https://mars.nasa.gov/all-about-mars/moons/summary/ (accessed 6.11.2023)

[48] "Tokamak", in: Max Planck Institute for Plasma Physics, no date, https://www.ipp.mpg.de/14869/tokamak (accessed 10.12.2023)

[49] N.J. Fisch, "Theory of Current Drive in Plasmas", *Reviews of Modern Physics* **1987**, *59*(1), p. 175–234, doi:10.1103/RevModPhys.59.175

[50] R.D. Leach, M.B. Alexander, "Failures and Anomalies Attributed to Spacecraft Charging", NASA Reference Publication 1375, **1995**

[51] A.V. Durrant, *Quantum Physics of Matter*, 1st Edition, CRC Press, Boca Raton, Fla., **2000**, p. 102–111

[52] Y. Ando, X. Zhao, T. Sugai, M. Kumar, "Growing carbon nanotubes", *Materials Today* **2004**, *7*(10), p. 22–29, doi:10.1016/S1369-7021(04)00446-8

[53] M. Bockrath, "The weakest link", *Nature Physics* **2006**, *2*, p. 155–156, doi:10.1038/nphys252

[54] Z. K. Tang et al., "Superconductivity in 4 Angstrom Single-Walled Carbon Nanotubes", *Science* **2001**, *292*, p. 2462–2465, doi:10.1126/science.1060470

[55] I. Takesue, J. Haruyamaand, N. Kobayashi, S. Chiashi, S. Maruyama, T. Sugai, H. Shinohara, "Superconductivity in Entirely End-Bonded Multiwalled Carbon Nanotubes", *Physics Review Letters* **2006**, *96*(5), 057001, doi:10.1103/PhysRevLett.96.057001

[56] Y. Zhang, X. Xu, "Yttrium barium copper oxide superconducting transition temperature modeling through gaussian process regression", *Computational Materials Science* **2020**, *179*, 109583, doi:10.1016/j.commatsci.2020.109583.

[57] E. Yanagisawa et al., "Properties of Pb-Doped Bi-Sr-Ca-Cu-O Superconductors", *Japanese Journal of Applied Physics* **1988**, *27*(8), L1460–1462, doi:10.1143/JJAP.27.L1460

[58] A.I. Golovashkin, O.M. Ivanenko, Y.B. Kudasov, K.V. Mitsen, A.I. Pavlovsky, V.V. Platonov, O.M. Tatsenko, "Low Temperature Direct Measurements of Hc2 in HTSC Using Megagauss Magnetic Fields", *Physica C: Superconductivity* **1991**, *189*, p. 1859–1860, doi:10.1016/0921-4534(91)91055-9.

[59] F.R. Fickett, "Standards for Measurement of the Critical Fields of Superconductors", *Journal of research of the National Bureau of Standards* **1985**, *90*(2), p. 95–113, doi.org/10.6028/jres.090.007

[60] K.H.J. Buschow et al., *Encyclopedia of Materials: Science and Technology*, 2nd Edition, Elsevier, Amsterdam, **2001**, p. 1–6, doi:10.1016/B0-08-043152-6/02023-4

[61] P. Tixador, "Advances in HTS materials", *WAMSDO Workshop Accelerator Magnet Superconductors, Design and Optimization* **2009**, p. 89–93, doi:10.5170/CERN-2009-001.89

[62] A.P. Malozemoff et al., "Progress in high temperature superconductor coated conductors and their applications", *Superconductor Science and Technology* **2008**, *21*, 034005, doi:10.1088/0953-2048/21/3/034005

[63] J. Hänisch et al., "Determination of the irreversibility field of YBCO thin films from pulsed high-field measurements", *Superconducting Science and Technology* **2007**, *20*, p. 228–231, doi:10.1088/0953-2048/20/3/019

[64] A. Knizhnik, G.E. Shter, G.S. Grader, G.M. Reisner, Y. Eckstein, "Interrelation of preparation conditions, morphology, chemical reactivity and homogeneity of ceramic YBCO", *Physica C: Superconductivity* **2003**, *400*(2), p. 25–35, doi:10.1016/S0921-4534(03)01311-X

[65] "Abundance of Elements in Earth's Crust", in: Wikipedia, last edited: 24.11.2023, https://en.wikipedia.org/w/index.php?title=Abundance_of_elements_in_Earth%27s_crust&oldid=1186702498 (accessed 25.11.2023)

[66] R.W. Fairbridge, C.P. Marshall, *Encyclopedia of Geochemistry*, 1st Edition, Springer, Dordrecht, **1999**, p. 145

[67] "Market Data", in: Westmetall, no date, https://www.westmetall.com/en/markdaten.php?action=table&field=LME_Cu_cash (accessed 28.11.2023)

[68] US Bureau of Economic Analysis, "Gross Domestic Product (Second Estimate), Corporate Profits (Preliminary Estimate), Third Quarter 2023", news release November 29th, 2023

[69] Z. Wang, H. Becker, "Chalcophile elements in Martian meteorites indicate low sulfur content in the Martian interior and a volatile element-depleted late veneer", *Earth and Planetary Science Letters* **2017**, *463*, p. 56–68, doi:10.1016/j.epsl.2017.01.023.

[70] V. Smolyaninova, K. Zander, T. Gresock et al. "Using metamaterial nanoengineering to triple the superconducting critical temperature of bulk aluminum", *Scientific Reports* **2015**, 15777, doi:10.1038/srep15777

[71] M.R. Shavers, N. Zapp, R.E. Barber, J.W. Wilson, G. Qualls, L. Toupes, S. Ramsey, V. Vinci, G. Smith, F.A. Cucinotta, "Implementation of ALARA radiation protection on the ISS through polyethylene shielding augmentation of the Service Module Crew Quarters", *Advances in Space Research* **2004**, *34*(6), p. 1333–1337, doi:10.1016/j.asr.2003.10.051

List of Figures

[Title] Bing Image Creator, https://www.bing.com/create, 3.12.2023, prompt: "Futuristic green city on Mars. Straight blue magnetic field lines in the whole sky, horizontal, horizontal, evenly spaced. Many plants and lakes. Empty sky"

[Figure 1] © Geek3, "Field of a cylindrical bar magnet computed accurately", **2010**, https://upload.wikimedia.org/wikipedia/commons/thumb/0/0c/VFPt_cylindrical_magnet_thumb.svg/640px-VFPt_cylindrical_magnet_thumb.svg.png (accessed 4.12.2023), modified under CC BY-SA 3.0 license (https://creativecommons.org/licenses/by-sa/3.0/deed)

[Figure 2] © Geek3, **2020**, https://upload.wikimedia.org/wikipedia/commons/thumb/2/2e/VFPt_dipoles_electric.svg/1024px-VFPt_dipoles_electric.svg.png (accessed 4.12.2023), modified under CC BY-SA 4.0 license (https://creativecommons.org/licenses/by-sa/4.0/)

[Figure 3] P.P. Urone, R. Hinrichs, K. Dirks, M. Sharma, *College Physics*, © OpenStax (Rice University), Houston, Tex., **2020**, p. 961, under CC BY 4.0 license (https://creativecommons.org/licenses/by/4.0/deed)

[Figure 4] P.P. Urone, R. Hinrichs, K. Dirks, M. Sharma, *College Physics*, © OpenStax (Rice University), Houston, Tex., **2020**, p. 963, under CC BY 4.0 license (https://creativecommons.org/licenses/by/4.0/deed)

[Figure 5] "Earth's Inconstant Magnetic Field", in: NASA Science, **2003**, https://web.archive.org/web/20230622182928/https://science.nasa.gov/science-news/science-at-nasa/2003/29dec_magneticfield/ (accessed 4.12.2023)

[Figure 6] © Geek3, **2006**, https://upload.wikimedia.org/wikipedia/commons/d/db/Toroidal_coord.png (accessed 4.12.2023), modified under CC BY-SA 3.0 license (https://creativecommons.org/licenses/by-sa/3.0/deed)

[Figure 7] © S. Li, H. Jiang, Z. Ren, C. Xu, "Optimal Tracking for a Divergent-Type Parabolic PDE System in Current Profile Control", *Abstract and Applied Analysis* **2014**, *2014*, 940965, doi:10.1155/2014/940965, modified under CC BY-SA 3.0 license (https://creativecommons.org/licenses/by-sa/3.0/deed)

[Figure 8] J. L. Green, J. Hollingsworth, D. Brain, V. Airapetian, A. Glocer, A. Pulkkinen, C. Dong, and R. Bamford, "A Future Mars Environment for Science and Exploration", *NASA's Planetary Science Vision 2050 Workshop* **2017**, LPI Contribution No. 1989

Additionally, the title picture and Figure 7 were upscaled with Pixelcut (https://create.pixelcut.ai/uscaler) on 3.12.2023, Figure 3 and Figure 4 on 2.12.2023.

Declaration of Authenticity

I confirm that I have independently written this paper and have cited all sources and aids. Any passages taken over verbatim or in essence are indicated for reference. I also confirm that the use of AI tools is accurately disclosed in accordance with the document "Ergänzende Hinweise zur Verwendung von KI-Tools bei Maturitätsarbeiten" (19.07.2023).